

# A Compact, Tri-band and Circularly Polarized Patch Antenna Using a Ferrite Material

S. Jemmeli<sup>1</sup>, T. Monediere<sup>1</sup>, E. Arnaud<sup>1</sup>, L. Huitema<sup>1</sup>

<sup>1</sup> UMR CNRS 7252, Université de Limoges, Xlim, 12 rue Gémini 87068 Limoges, France

sarra.jemmeli@xlim.fr

**Abstract**— A single fed, compact and circularly polarized patch antenna operating in three frequency bands is proposed in the present paper. This patch antenna uses a polarized ferrite substrate which therefore has the property of naturally generating circularly polarized waves. The modelling process of a compact antenna having dimensions of  $\frac{\lambda_0}{3.3} \times \frac{\lambda_0}{3.3} \times \frac{\lambda_0}{153.9}$  at 3GHz and presenting three circularly polarized modes is exhibited. A prototype measurement has been carried out for an experimental validation of the simulated results.

**Index Terms**— Saturated ferrite materials, circular polarization, compactness, tri-band operation.

## I. INTRODUCTION

Due to the rapid development of wireless communication systems, antennas, as fundamental components of these systems, are playing a crucial role on their performances enhancement. Indeed, many military and space applications require multi-band antennas with circular polarization. These objectives are often difficult to achieve while in addition the antennas must be miniaturized.

The design of a dual-band circularly polarized antenna has been covered in many studies. Several techniques have been reported to achieve such radiation while using a single feeding probe, such as implementing slots [1]-[2] or truncating the radiating element corners [3]. Another method to obtain a dual-band operation while generating circularly polarized modes is to use multiple feeding probes or a feeding network [4]-[5]. However, the use of power dividers or hybrid couplers necessary for the implementation of these feeding techniques induces additional losses affecting performances of the antennas. In the literature, only few papers have addressed the problem of low profile, circularly polarized and tri-band antennas. Basically, the most of the proposed antennas present a complex geometry and the miniature criterion is seldom addressed. Indeed, in [6], the authors discussed a tri-band circularly polarized antenna working at 1.3GHz, 1.98GHz and 3GHz. The first and the third modes are generated by a central patch including four T-shaped slits while the second frequency band is generated by a second radiating element surrounding the first patch and fed through another feeding element. However, this device presents a dimension of  $\frac{\lambda_0}{3.3} \times \frac{\lambda_0}{3.3} \times \frac{\lambda_0}{153.9}$  on its first operating frequency. In another study [7], a stacked patch antenna is proposed in order to have the tri-band operation. The structure consists of three radiating elements. The upper patch is fed through a single probe and the two others by

electromagnetic coupling. The geometry of the upper and the middle radiating elements is modified by truncating their corners. Two symmetry I-slot are also added to the middle patch, a slit is integrated into the lower radiating element in order to achieve the circular polarization behavior. The device presents a good polarization quality since the axial ratio at the three operating frequencies are respectively of 1.54dB, 0.68dB and 0.59dB at 1.176GHz, 1.227GHz and 1.575GHz. But the antenna size is about  $\frac{\lambda_0}{3.8} \times \frac{\lambda_0}{3.8} \times \frac{\lambda_0}{53.1}$  at the first operating frequency.

In the current work, an appropriate solution to acquire a good circular polarization and a tri-band operation while having a miniature antenna, is addressed. A ferrite material is used as substrate. Ferrite materials, when they are polarized by a static magnetic field, are able to generate circularly polarized modes (RHCP and LHCP) at different frequencies [8], even if the antenna is excited through a single probe feed. In addition, due to the need for miniaturization, ferrites are an interesting solution to reduce the size of antennas since they have a permeability greater than 1 combined to a high permittivity. Various studies have been reported in the literature on ferrite antennas [9], but with few experimental results. Moreover, the different steps of modelling a ferrite antenna are usually not presented. A particularly important step, generally not dealt in the literature, is the accurate determination of the static magnetic field in the ferrite which is generated by the permanent polarization magnets, however, this is an essential point to master the operation of the antenna.

In the present paper, the complete design of a miniature, circularly polarized patch antenna working in three frequency bands, fed through a single coaxial cable and based on a polarized ferrite material is exhibited. The paper is divided into three parts. Section II is dedicated to the presentation of the main ferrite materials properties. Section III describes the geometry and the modelling process of the ferrite patch antenna. The device behavior is evaluated through simulations using the software CST Microwave Studio [10]. The antenna performances in terms of radiation efficiency ( $\eta_{rad}$ ), axial ratio ( $AR$ ) and reflection coefficient ( $|S_{11}|$ ) are analyzed. The experimental study is developed in section IV, where the simulation results are validated through a prototype measurement.

## II. FUNDAMENTAL SATURATED FERRITE MATERIALS CHARACTERISTICS

The non-reciprocal behavior of saturated ferrite materials, under a continuous (DC) magnetic field biasing, is given by a permeability tensor called Polder tensor described by (1) [8]:

$$[\mu_r(\omega)] = \begin{bmatrix} \mu & -j\kappa & 0 \\ j\kappa & \mu & 0 \\ 0 & 0 & 1 \end{bmatrix} \quad (1)$$

The permeability tensor elements are given by:

$$\mu = 1 + \frac{\omega_m \omega_0}{\omega_0^2 - \omega^2} = \mu' - j\mu'' \quad (2)$$

$$\kappa = \frac{\omega_m \omega}{\omega_0^2 - \omega^2} = \kappa' - j\kappa'' \quad (3)$$

Where:  $\omega = 2\pi f$ ,  $\omega_m$  is the gyrotropic frequency defined by  $\omega_m = \gamma\mu_0 M_s$  and  $\omega_0$  the Larmor frequency given by  $\omega_0 = \gamma\mu_0 H_i + j\omega\alpha$ .

The Polder tensor elements (2) - (3) depend basically on the frequency  $f$ , the internal magnetic field  $H_i$  and the saturation magnetization  $M_s$  of the material [8]. This permeability tensor considers also the magnetic losses given by the damping factor  $\alpha = \frac{\gamma\Delta H}{2f}$  where  $\Delta H$  is the ferrite line width.

To define ferrite antennas operating areas, another important parameter has to be introduced which is the effective permeability expressed by (4):

$$\mu_{eff} = \frac{\mu^2 - \kappa^2}{\mu} \quad (4)$$

The different Polder tensor elements (2) - (3) and the effective permeability (4) are plotted in Fig.1. From this figure, two zones can be distinguished: the strong and the weak field area. The strong field area is defined for frequencies lower than the gyromagnetic resonance, which occurs when the precession frequency reaches the Larmor frequency, as to the weak field area defined for frequencies higher than this resonance.

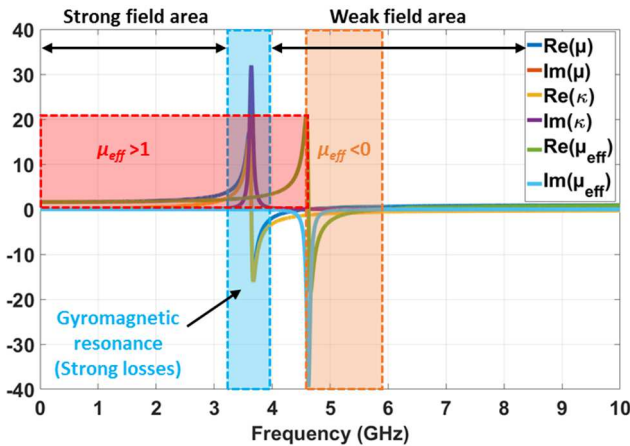


Fig. 1. Polder's parameters versus the frequency for Y39 ferrite material with  $H_i=1300\text{Oe}$ ,  $\epsilon_r=14.6$ ,  $\tan\delta=2\times 10^{-4}$ ,  $4\pi M_s=800\text{Gauss}$  and  $\Delta H_{eff}=4\text{Oe}$ .

The proposed antenna geometry will be optimized to generate three working frequencies. The two first modes will

be in the strong field area and the third mode in the weak field area far away from the gyromagnetic resonance, where the material presents high losses. Since the ferrite presents a high permeability in the strong field area, the antenna will be miniature in this zone.

Our work is a proof of concept, not dedicated for a defined application. Thus, the operating frequencies are chosen, arbitrarily, through a preliminary "Eigen mode" study considering the ferrite patch antenna as a cylindrical cavity. The device wave equation, depending on its radius and the ferrite substrate magnetic characteristics, is solved and the operating frequencies are deduced for a specified internal magnetic field [8].

## III. SIMULATIONS RESULTS

The design of the antenna involves three essential steps:

- The first consists in an electromagnetic analysis/simulation in which the static magnetic field in the ferrite material is assumed to be "ideal and constant". The working frequencies are then calculated.
- The second consists of a magnetic study which makes it possible to choose the permanent magnets allowing to obtain in practice the wanted static magnetic field (calculated in the first step).
- The third one combines electromagnetic and magneto-static co-simulation.

### A. Modelling process of a ferrite patch antenna

In the first step a ferrite antenna is modelled with a uniform magnetic field ( $H_i=1300\text{Oe}$ ) inside the ferrite substrate (ideal case study). Three resonant frequencies are obtained. The designed antenna configuration is described in Fig.2. The proposed design is based on a rectangular ferrite substrate Y39 (Yttrium - Aluminum) of  $10,5\text{mm}\times 10\text{mm}\times 3\text{mm}$  fed by a single coaxial probe. The dimensions of the square ground plane are  $20\text{mm}\times 20\text{mm}$ . The antenna radiating element and the ground plane are both composed of two stacked metallized ROGERS (RO4003C) plates to facilitate the soldering of the coaxial cable. Other fabrication constraints are also added to the antenna structure to better evaluate its performances (soldering, the lower magnet hole diameter ...). As the internal magnetic field in the real case is provided by permanent magnets, the next step therefore consists in evaluating the homogeneity of the generated magnetic field polarizing the ferrite substrate. Two commercial magnets are added to the structure. The upper one is rectangular Neodymium N45 ( $B_{r1}=1.35\text{T}$ ,  $t_1=1.1\text{mm}$ ,  $\mu_{r1}=1.2$ ) placed on the top of the radiating element and the lower one is cylindrical Neodymium N35 ( $B_{r2}=1.2\text{T}$ ,  $t_2=6.4\text{mm}$ ,  $\mu_{r2}=1.1$ ) integrated under the ground plane. To further homogenize the internal magnetic field, two steel plates were inserted between the magnets and the antenna elements.

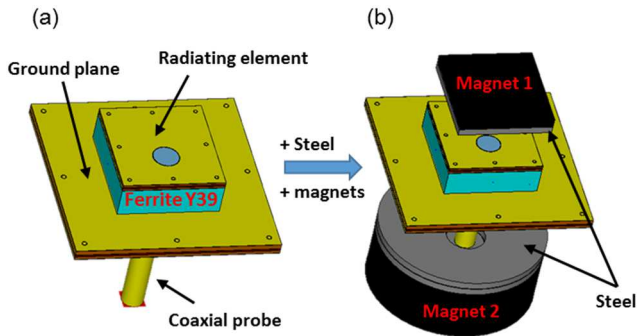


Fig. 2. Antenna design (a) in the ideal case study and (b) in the real case study.

The 3D distribution of the magnetic field inside the ferrite material is presented in Fig.3 (a) and the evolution of the internal field along  $x$  and  $y$  axis in the middle of the substrate is depicted in Fig.3 (b). According to these figures, the internal magnetic field  $H_i$  is quite uniform in the middle of the ferrite and presents an average value of 1310Oe. In the vicinity of the feeding probe, the  $H_i$  is lower than the target value due to the hole piercing, but all the antenna parameters were adjusted and well optimized to avoid the performances distortions.

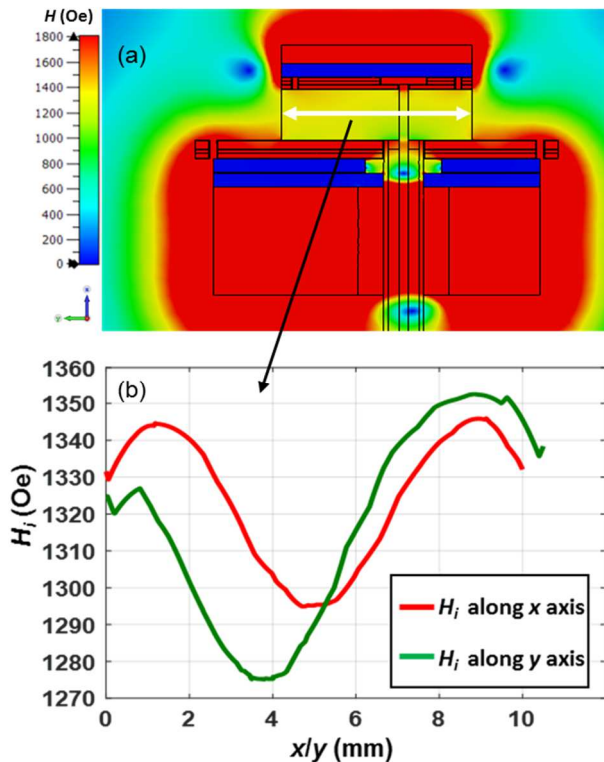


Fig. 3. 3D internal magnetic field cartography (a), evolution of  $H_i$  in the middle of the ferrite substrate along  $x$  and  $y$  axis (b).

### B. Comparison between ideal and real cases results

The antenna configuration illustrated in Fig.2 (a), is computed in the ideal case, while the internal magnetic field is homogenous and of 1300Oe. To validate this analysis and before realizing a prototype, a “real case” study has to be

carried out (electromagnetic and magnetostatic co-simulation with CST), that is to say when the biasing field is that evaluated through the magnetostatic study. The antenna given by Fig.2 (b) is therefore simulated.

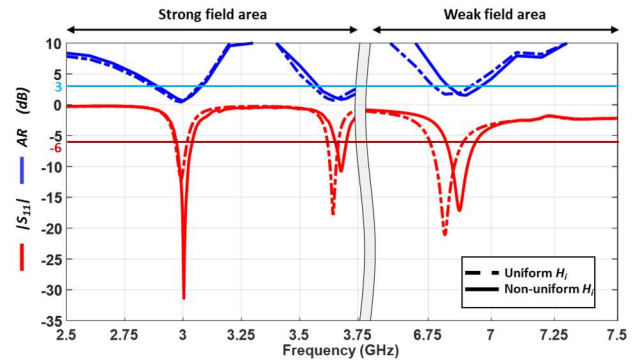


Fig. 4.  $|S_{11}|$  parameter and axial ratio of the designed patch antenna considering a uniform and non-uniform internal magnetic field.

A comparative study of the antenna performances in terms of axial ratio and reflection coefficient is established in Fig.4. According to this figure, in the strong field area, two counter-rotating modes  $TM_{-11}$  and  $TM_{+11}$  are excited within the antenna in both cases, the first one is a right-handed circular polarization and the second one is a left-handed circular polarization. In the weak field area, a third mode with a right-handed circular polarization appears. The antenna is well matched on the three frequencies since the  $|S_{11}|$  is lower than  $-6\text{dB}$  (a fixed criterion for miniature antennas). To further evaluate the antenna performances and the effect of the non-homogenous internal field, a comparative table (Table I) illustrating the working frequencies, the axial ratio, the radiation efficiency and the antenna dimensions on each mode and in both cases, is addressed.

TABLE I. COMPARISON BETWEEN THE ANTENNA PERFORMANCES IN THE IDEAL AND REAL CASE STUDY

|                                                                         | Ideal case study                                                                                                                                                                                                                                            | Real case study                                                                                                                                                                                                                                           |
|-------------------------------------------------------------------------|-------------------------------------------------------------------------------------------------------------------------------------------------------------------------------------------------------------------------------------------------------------|-----------------------------------------------------------------------------------------------------------------------------------------------------------------------------------------------------------------------------------------------------------|
| <b>Working frequencies <math>f_w</math></b>                             | 2.99GHz<br>3.64GHz<br>6.82GHz                                                                                                                                                                                                                               | 3GHz<br>3.68GHz<br>6.87GHz                                                                                                                                                                                                                                |
| <b>AR (<math> S_{11}  &lt; -6\text{dB}</math>)</b>                      | <1.1dB<br><1dB<br><3.5dB                                                                                                                                                                                                                                    | <1.5dB<br><1.2dB<br><3.3dB                                                                                                                                                                                                                                |
| <b><math>\eta_{rad}</math> (<math> S_{11}  &lt; -6\text{dB}</math>)</b> | >80%<br>>80%<br>>85%                                                                                                                                                                                                                                        | >60%<br>>70%<br>>80%                                                                                                                                                                                                                                      |
| <b>Antenna dimensions</b>                                               | $\frac{\lambda_0}{10} \times \frac{\lambda_0}{9.6} \times \frac{\lambda_0}{27}$<br>$\frac{\lambda_0}{8.3} \times \frac{\lambda_0}{7.9} \times \frac{\lambda_0}{22.2}$<br>$\frac{\lambda_0}{4.4} \times \frac{\lambda_0}{4.2} \times \frac{\lambda_0}{11.9}$ | $\frac{\lambda_0}{10} \times \frac{\lambda_0}{9.5} \times \frac{\lambda_0}{27}$<br>$\frac{\lambda_0}{8.2} \times \frac{\lambda_0}{7.8} \times \frac{\lambda_0}{22}$<br>$\frac{\lambda_0}{4.4} \times \frac{\lambda_0}{4.2} \times \frac{\lambda_0}{11.8}$ |

Comparing the working frequencies, a slight frequency shift can be seen due to the non-homogeneity of the internal magnetic field in some ferrite areas as explained in the magnetostatic study. To evaluate the circular polarization quality, we consider the axial ratio. It is obvious that the antenna presents a good circular polarization on the two first frequency bands since the axial ratio ( $AR$ ) is lower than 3dB on the matching bands. On the third mode, the  $AR$  is not as low as for the two other modes due to the thickness of the ferrite substrate at this frequency, however, it remains quite satisfying. Regarding the radiation efficiency ( $\eta_{rad}$ ) when the  $|S_{11}|$  is lower than -6dB, the antenna radiates more than 80% of the accepted power on the first and the second modes in the ideal case. As to the third mode, the  $\eta_{rad}$  is higher than 85% because the antenna is not miniature in this area. In the real case study, the antenna radiation efficiency has been decreased in the strong field area since the device radiates more than 60% on the first mode and 70% on the second one. This reduction could be explained by the fact that in some areas of the ferrite material, especially in the vicinity of the feeding probe, the two first modes are very close to the gyromagnetic resonance increasing the magnetic losses inside the ferrite substrate. The antenna dimensions are therefore calculated as a function of the wavelength to characterize the device size. The reported dimensions confirm the fact that the antenna is miniature in the strong field area, in both cases.

#### IV. PROTOTYPE MEASUREMENT RESULTS

Once the antenna behavior is investigated, an experimental validation has to be carried out through a prototype measurement. The antenna elements are assembled and aligned by a Rohacell support. The feeding coaxial cable is soldered to the ground plane and to the radiating element. The prototype is therefore measured in the anechoic chamber (Fig.5).

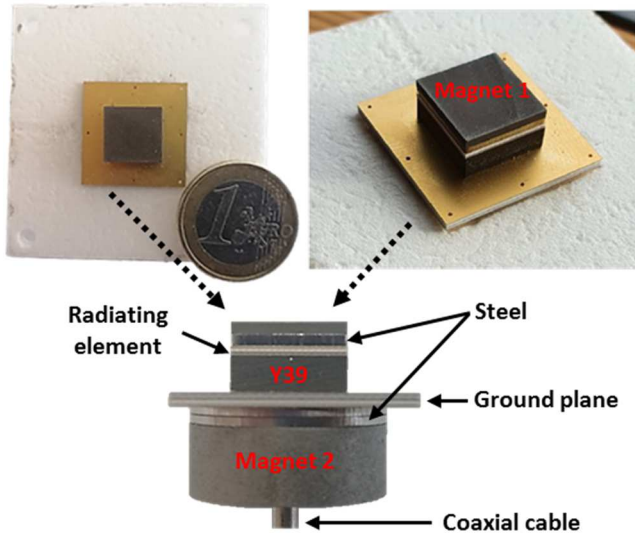


Fig. 5. The measured antenna configuration

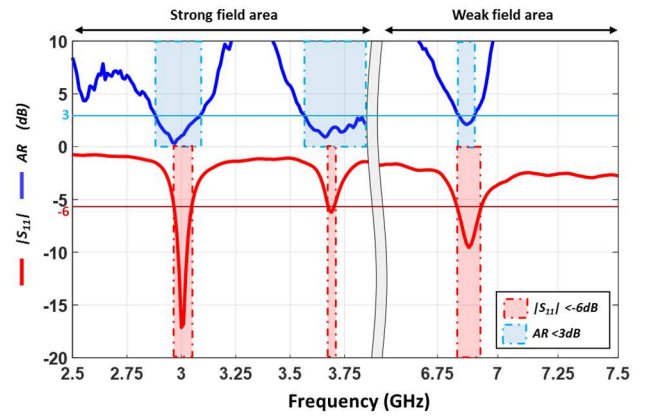
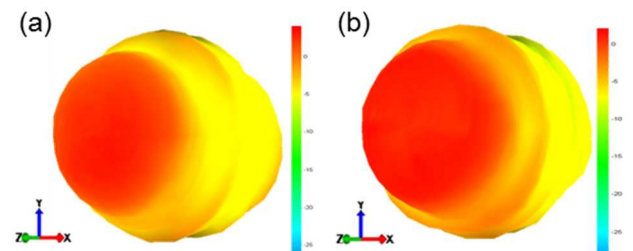


Fig. 6. The measured  $|S_{11}|$  parameter and axial ratio versus the frequency.

Considering the  $|S_{11}|$  and axial ratio measured and depicted in Fig.6, it can be observed that we retrieve the three modes at 3GHz, 3.69GHz and 6.88GHz, respectively. A good agreement between the measured and the simulated frequencies is noticed. The axial ratio plot shows that the antenna presents a good boresight circular polarization. In fact, it is lower than 2.1dB and 1.84dB for the two first working bands, respectively. As to the third band, the axial ratio remains under 3.6dB where the  $|S_{11}|$  is lower than -6dB. At the central frequencies and for  $\theta=\phi=0^\circ$ , the axial ratio is about 1dB, 1.68dB and 2.1dB, respectively.

The measured realized gain radiation patterns at the three working frequencies are plotted in Fig.7. We can notice from these figures that the radiation patterns have a boresight direction as a conventional patch antenna. The measured realized gain and the directivity on each working frequency are extracted and exhibited in Table II. We can see that the antenna can achieve a realized gain of 3.61dB, 1.82dB and 6.5dB at the three central frequencies. From the directivity (6dBi, 6.3dBi and 7.4dBi, respectively) and the reflection coefficient at each working frequency, we can calculate the radiation efficiency of the antenna. The antenna radiates 59% of the accepted power on the first mode at 3GHz and 50% on the LHCP mode at 3.69GHz. For the third mode at 6.88GHz, the radiation efficiency is about 92%. Considering the mismatching losses, the antenna total efficiencies are about 58%, 36% and 81% on the three modes respectively.



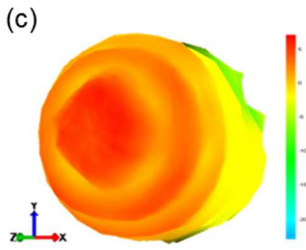


Fig. 7. The measured realized gain radiation patterns at 3GHz (a), 3.69GHz (b) and 6.88GHz (c).

As to the antenna dimensions, the device presents a size of  $\frac{\lambda_0}{10} \times \frac{\lambda_0}{9.5} \times \frac{\lambda_0}{27}$  at 3GHz,  $\frac{\lambda_0}{8.1} \times \frac{\lambda_0}{7.7} \times \frac{\lambda_0}{22}$  at 3.69GHz and  $\frac{\lambda_0}{4.4} \times \frac{\lambda_0}{4.2} \times \frac{\lambda_0}{11.8}$  at 6.88GHz which confirms that the antenna is quite miniature in the strong field area.

TABLE II. THE PROTOTYPE MEASUREMENT RESULTS

| $f_w$    | Realized gain | Directivity | $\eta_{rad}$ | $\eta_{total}$ |
|----------|---------------|-------------|--------------|----------------|
| 3 GHz    | 3.61dB        | 6dBi        | 59%          | 58%            |
| 3.69 GHz | 1.82dB        | 6.3dBi      | 50%          | 36%            |
| 6.88 GHz | 6.5dB         | 7.4dBi      | 92%          | 81%            |

## V. CONCLUSION

The purpose of this paper is to take advantage of ferrite material intrinsic properties to implement, for the first time, a tri-band miniature and circularly polarized patch antenna. The antenna performances were investigated considering the magnetic field homogeneity inside the ferrite substrate. The simulated results were therefore validated through a prototype measurements.

## ACKNOWLEDGMENT

This work has been carried out in the framework of a joint laboratory INOGYRO between the SME Inoveos and the XLIM Laboratory.

## REFERENCES

- [1] A. A. Heidari, M. Heyrani and M. Nakhkash, "A Dual-band Circularly Polarized Stub Loaded Microstrip Patch Antenna for GPS Applications", *Progress In Electromagnetics Research, PIER*, vol. 92, pp. 195-208, 2009.
- [2] K. S. Rao, D. R. Jahagirdar and D. Ramakrishna, "Compact Broadband Asymmetric Slit Circularly Polarized Microstrip Patch Antenna for GPS and GLONASS Applications", *IEEE International Conference on Antenna Innovations & Modern Tech. for Ground, Aircraft and Satellite Applications (iAIM)*, Nov. 2017.
- [3] Z. N. Chen, X. Qing and H. L. Chung, "A Universal UHF RFID Reader Antenna", *IEEE Tans. On Microwave Theory and Tech.*, vol. 57, no. 5, pp. 1275-1282, May 2009.
- [4] D. M. Pozar and S. M. Duffy, "A Dual-Band Circularly Polarized Aperture-Coupled Stacked Microstrip Antenna for Global Positioning Satellite", *IEEE Trans. Antennas Propag.*, vol.45, no.11, Nov. 1997.

- [5] F. Bilotti and C. Vegni, "Design of High-Performing Microstrip Receiving GPS Antennas With Multiple Feeds", *IEEE Antennas and Wireless Propag. Lett.*, vol.9, May 2010.
- [6] Y. Jie, L. Chunlan and S. Juhong, "Design of Compact Multi-band Circularly-polarized Microstrip Antenna", *IEEE Proc. Antenna & Propag. China*, Oct. 23-25 2013.
- [7] O. P. Falade, M. U. Rehman, Y. Gao, X. Chen and C. G. Parini, "Single Feed Stacked Patch Circular Polarized Antenna for Triple Band GPS Receivers", *IEEE Trans. on Antennas and Propag.*, vol. 60, No. 10, pp. 4479-4484, Oct. 2012.
- [8] D. M. Pozar, "Radiation and Scattering Characteristics of Microstrip Antennas on Normally Biased Ferrite Substrates", *IEEE Trans. Antennas Propag.*, Vol. 40, no. 9, pp. 1084-1092, Sept. 1992.
- [9] M. Mashhadi, N. Komjani, B. Rejaei and J. Ghalibafan, "Ferrite-based Wideband Circularly Polarized Microstrip Antenna Design", *ETRI Journal*, vol. 41, no 3, pp. 289-297, 2019.
- [10] CST Microwave Studio, www.3ds.com